J. Chem. Sci. (2018) 130:126
https://doi.org/10.1007/s12039-018-1529-x
© Indian Academy of Sciences

REGULAR ARTICLE

A tetranuclear iron complex: substitution with triphenylphosphine ligand and investigation into electrocatalytic proton reduction

MOOKAN NATARAJAN, VISHAKHA KAIM, NAVEEN KUMAR and SANDEEP KAUR-GHUMAAN*
Department of Chemistry, University of Delhi, Delhi 110 007, India
E-mail: skaur@chemistry.du.ac.in

MS received 24 April 2018; revised 8 June 2018; accepted 24 July 2018; published online 3 September 2018

Abstract. The reaction of the tetranuclear iron complex [μ_4-Sulfido-bis{(μ-2-furylmethanethiolato) bis[tricarbonyliron](Fe—Fe)}] **1** with PPh_3 was explored. The reaction leads to the formation of the mono-substituted complex [Fe_2(μ-2-furylmethanethiolate)$_2$(CO)$_5$(PPh_3)] **2**. X-ray crystal structure has been reported for complex **2**. Complexes **1** and **2** were found to be active catalysts for proton reduction. Complexes **1** and **2** showed comparable catalytic activity for proton reduction to dihydrogen.

Keywords. Hydrogenases; catalysis; iron carbonyl complexes; proton reduction; monodentate phosphine.

1. Introduction

Hydrogen is being considered as a potential energy vector for the future as its combustion produces energy and only water as the by-product. Generation of hydrogen is, therefore, a clean alternative to fossil fuels. In nature, the [FeFe] hydrogenase enzyme is capable of reversibly and rapidly catalyzing hydrogen evolution and oxidation.[1] The active site (H-cluster) of this metalloenzyme, as revealed by the crystal structure investigations a decade ago, consists of one [4Fe4S] cubane and one [2Fe2S] subunit (Figure 1).[2,3] In the [2Fe2S] subunit, the two iron atoms are linked by a dithiolate ligand, in addition to co-ordination with CO and CN^- ligands.[2–5] Since the revelation of the detailed structural information of the enzyme active site, there has been tremendous interest in the study of organometallic model complexes of the H-cluster, in order to develop cheap, efficient and inexpensive catalysts for the production of dihydrogen.[1,6,7] Dithiolate-bridged complexes of the type **I** have been reported with a wide variety of terminal ligand (CO, CN^-, PR_3, NHCs, etc.) combinations (Figure 1).[8] Though many complexes of type **I** are known, there are not many reports of monothiolate-bridged complexes i.e., type **II**. A few selected examples reported are: [Fe_2(μ-napthalene-2-thiolate)$_2$(CO)$_5$L] (L = CO, PPh_3);[9a] [Fe_2(μ-*p*-toluenethiolate)$_2$(CO)$_6$], [Fe_2(μ-CH_2Ph)$_2$(CO)$_6$];[9b] [Fe_2(μ-SCH_2-*o*-C_6H_4OX)$_2$(CO)$_6$] (X = H, Me);[10] [Fe_2(CO)$_6$(μ-SC_6H_4-R)$_2$ (R = *p*-H, *o*-CH_3O, *p*-CH_3O, *p*-Cl)];[11] [Fe_2(CO)$_4$(μ-SC_6H_4-*o*-CH_3O)$_2$(PMe_3)$_2$];[10] [μ-S-2-RCONHC_6H_4)$_2$$Fe_2(CO)_6$] (R = Me, CF_3, Ph, 4-F-C_6H_4);[12] [Fe_2(μ-SEt)$_2$(CO)$_6$];[13] [Fe_2(μ-SEt)$_2$(CO)$_4$(PMe_3)$_2$];[12] [Fe_2(μ-SR)$_2$(CO)$_6$] (R = 2-thienyl, 2-thienylmethyl,2-$C_4H_3SCH_2$);[14] [Fe_2(μ-SMe)$_2$(CO)$_6$];[15] [Fe_2{μ-$SCH_2CH(OH)CH_2$(OH)}$_2$(CO)$_6$];[16] [Fe_2(μ-SPh)$_2$(CO)$_6$];[17] [Fe_2(μ-CH_2 CH_2CH_2OH)$_2$(CO)$_6$];[18] [Fe_2(CO)$_4$(μ-SEt)$_2$(CN)$_2$];[19] [Fe_2(μ-SC_6H_2-^{i}Pr_3-2, 4, 6)$_2$(CO)$_6$];[20] [Fe_2(μ-SC_6H_2 Me_3-2, 4, 6)$_2$(CO)$_6$],[19] etc. Most of the above complexes have been reported as structural models of the H-cluster. A few of the complexes [Fe_2(μ-napthalene-2-thiolate)$_2$(CO)$_5$L] (L = CO, PPh_3);[9a] [Fe_2(μ-*p*-toluenethiolate)$_2$(CO)$_6$];[9b] [Fe_2(μ-CH_2Ph)$_2$(CO)$_6$];[9b] [Fe_2(μ-SCH_2-*o*-C_6H_4OX)$_2$(CO)$_6$] (X = H, Me),[10] [Fe_2(CO)$_6$(μ-SC_6H_4-R)$_2$] (R = *p*-H, *o*-CH_3O, *p*-CH_3O, *p*-Cl),[11] [Fe_2(CO)$_4$(μ-SC_6H_4-*o*-OCH_3)$_2$(PMe_3)$_2$];[10] [μ-S-2−RCONHC_6H_4)$_2$$Fe_2(CO)_6$] (R = Me, CF_3, Ph, 4-F-C_6H_4);[12] [Fe_2(μ-SEt)$_2$(CO)$_6$];[13] [Fe_2(μ-SEt)$_2$(CO)$_4$(PMe_3)$_2$];[12] [Fe_2(μ-SMe)$_2$(CO)$_6$];[15] have been reported as catalysts for proton reduction in the presence of

*For correspondence

Electronic supplementary material: The online version of this article (https://doi.org/10.1007/s12039-018-1529-x) contains supplementary material, which is available to authorized users.

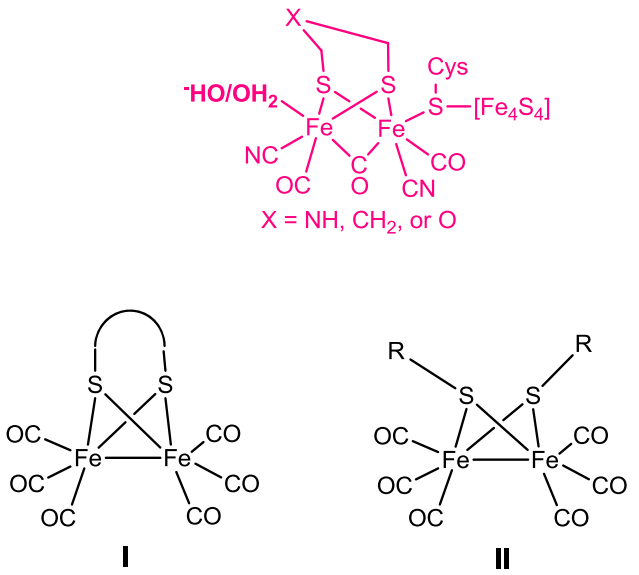

Figure 1. [FeFe] hydrogenase enzyme active site (top) and model complexes reported (bottom).

acids with low currents and high over potentials. Therefore, with an aim to further understand the influence of monothiolate ligands in the model complexes, the reported tetra iron precursor complex μ_4-Sulfido-bis {(μ-2-furylmethanethiolato) bis[tricarbonyliron] (Fe–Fe)} **1** was used to synthesize the monodentate phosphine substituted complex [Fe_2(μ-2-furylmethanethiolate)$_2$$(CO)_5(PPh_3)$] **2** (L = PPh_3).[21] The catalytic aspects of both the complexes (**1** and **2**) were investigated in the presence of acids of varying strengths by electrochemical investigations.

2. Experimental

2.1 *Materials and physical measurements*

All the experiments were carried out under an inert atmosphere using Schlenk line techniques. The reagents $Fe_3(CO)_{12}$, 2-furylmethanethiolate, triphenylphosphine, deuterated ($CDCl_3$) and anhydrous solvents (dichloromethane, tetrahydrofuran, acetonitrile) were obtained from Sigma-Aldrich and used without further purification. The precursor complex μ_4-Sulfido-bis{(μ-2-furylmethanethiolato)bis[tricarbonyliron](Fe—Fe)} **1** was prepared according to the procedure reported in literature.[21] The ^{1}H and ^{31}P {^{1}H} NMR spectra were recorded at room temperature in $CDCl_3$ solution with Jeol 400 MHz NMR spectrometer. The FTIR spectra were recorded from dichloromethane and acetonitrile solutions of the samples over the range 400−4000 cm^{-1} on a Perkin Elmer FTIR Spectrometer. The UV-Vis spectra for complexes were recorded on a Perkin-Elmer Lambda-25 spectrophotometer. Electrochemical measurements were conducted in acetonitrile with 0.1 M tetrabutylammonium hexafluorophosphate (Sigma-Aldrich, electrochemical grade) as supporting electrolyte that was dried in vacuum at 383 K. Cyclic voltammetry was carried out using an Autolab potentiostat with a GPES electrochemical interface. The working electrode was a glassy carbon disc (diameter 3 mm, freshly polished) for cyclic voltammetry. Platinum was used as the counter electrode. The reference electrode was a non-aqueous Ag/Ag^+ electrode (CH Instruments, 0.01 M $AgNO_3$ in acetonitrile). All the potentials are quoted against the ferrocene–ferrocenium couple (Fc/Fc^+); ferrocene was added as an internal standard at the end of the experiments. For the electrochemical measurements, all solutions were prepared from dry acetonitrile (Sigma-Aldrich, spectroscopic grade, dried with molecular sieves 3 Å).

2.2 *Synthesis of [Fe_2(μ-2-furylmethanethiolate)$_2$ $(CO)_5(PPh_3)$] **2***

The tetranuclear all carbonyl precursor complex **1** was synthesized as reported in literature.[21] A tetrahydrofuran solution of **1** (600 mg, 0.733 mmol) and the phosphine ligand (PPh_3) (192 mg, 0.733 mmol) were refluxed under argon atmosphere for 3 h. The resulting solution was evaporated to dryness under vacuum and the residue was chromatographed on a silica gel column. Elution with a mixture of hexane/dichloromethane (4:1, v/v) afforded an orange-red solution. Complex **2** was obtained as an air-stable orange-red powder after removal of the solvent. The complex was then recrystallized from hexane-dichloromethane solution by slow evaporation at – 4 °C. **1**: IR (CH_2Cl_2, cm^{-1}): 2070 (s), 2027 (s), 1968 (br).

2.2a *Complex* **2***:* [Fe_2(μ-2-*furylmethanethiolate*)$_2$ $(CO)_5(PPh_3)$]: Yield: 79.2% (0.772 g); IR (CH_2Cl_2, cm^{-1}): $\nu_{C=O}$ 2041 (s), 1979 (br), 1960 (s), 1926 (s); ^{1}H NMR (400 MHz, 298 K, ppm in $CDCl_3$): 7.70–7.30 (m, 15H, PPh_3), 6.22–5.78 (6H, furyl-H) 3.43–2.81 (4H, -CH_2-). ^{31}P NMR (161.8 MHz, 298 K, ppm in $CDCl_3$): 59.8 ppm (s, PPh_3).

2.3 *X-ray crystal structure analysis*

Single crystals for complexes **1** and **2** were grown by slow evaporation of hexane/dichloromethane solutions. X-ray data of the complexes were collected on an Oxford Xcalibur CCD single-crystal X-ray diffractometer at 293 K, equipped with graphite monochromatic MoK_α radiation (λ 0.71073 Å). Significant crystallographic parameters and refinement details for complex **2** are listed in Table 1. For details of complex **1,** see Supplementary Information. The crystal structures of the complexes were solved by direct methods using SIR-92 and refined by full-matrix least squares refinement techniques on F^2 using SHELXL-97.[22,23] The structure was solved and refined by standard procedures. The multi-scan absorption correction was applied. The coordinates of non-hydrogen atoms were refined anisotropically using SHELXL-

97.[24] All calculations were done using the Wingx software package.[25] For the molecular graphics, the program ORTEP-3 was used.[26]

3. Results and Discussion

3.1 *Synthesis and characterization*

The tetranuclear all carbonyl iron precursor complex μ_4-Sulfido-bis {(μ-2-furylmethanethiolato)bis[tricarbonyliron](Fe–Fe)} **1** was synthesized as reported in literature.[21] The reaction of precursor complex **1** with PPh_3 in refluxing THF afforded the target complex [Fe_2(μ-2-furylmethanethiolate)$_2$(CO)$_5$(PPh_3)] **2** in 79.2% yield (Scheme 1). Recrystallization from hexane and dichloromethane solutions at low temperature afforded orange-red crystals for complex **2**.

3.2 *Structure of the complexes*

3.2a *Crystal structure of* **2**: The molecular structure for **2** was confirmed by single crystal X-ray diffraction analysis (Figure 2, Tables 1 and 2). The Fe–Fe bond distance in complex **2** is 2.5207(4) Å which is close to that reported for the [FeFe] hydrogenase enzyme active site (2.6 Å).[2,3,27] The Fe–Fe bond distances in the reported complex **1** are Fe(1)–Fe(2), 2.5263(10) and Fe(3)–Fe(4), 2.5377(10) Å, which are only slightly higher than the Fe–Fe bond distance in complex **2** probably due to the bridging sulphide between the iron centers (see Supplementary Information).[21] The replacement of one CO ligand with the phosphine ligand in complex **2** has only a small effect on the Fe–Fe bond distance. The phosphine ligand occupies the apical position in **2** and the [2Fe2S] site is in butterfly conformation, with the equatorial-axial spatial orientation of the furylthiolate groups tethered to the iron centers.[9] The equatorial-axial spatial orientation is due to the presence of a monodentate phosphine ligand on one of the iron centers. This orientation has also been observed for similar complexes reported earlier.[9] The crystal packing along a axis showed two molecules present together (Figure S2, Supplementary Information). Intermolecular bonding for the complex was seen between C29–H29···O1 and C20–H20···O7 with bond distances of 2.551 and 2.612 Å, respectively (Figure S3, Supplementary Information).

Table 1. Crystallographic parameters and refinement details for complex **2**.

Empirical formula	$C_{33}H_{25}Fe_2O_7PS_2$
Formula weight	740.36
Crystal size (mm)	0.270 × 0.260 × 0.250
Temperature (K)	293(2)
Wavelength (Å)	0.71073
Crystal system	Triclinic
Space group	$P\bar{1}$
a (Å)	9.0095(4)
b (Å)	11.8668(8)
c (Å)	16.8481(10)
α (°)	70.847(6)
β (°)	84.436(4)
γ (°)	76.716(5)
V (Å^3)	1655.60(18)
Z	2
ρ_{calcd} (g cm^{-3})	1.485
Absorption coefficient (mm^{-1})	1.096
Two theta range for data collection (°)	6.42 to 58.82
Refinement method	Full-matrix least-squares on F^2
No. of unique reflns (R_{int})	8022 (0.0257)
Index ranges	$-12 \le h \le 11, -16 \le k \le 15, -22 \le l \le 23$
F_{000}	1010
$R_1[I > 2\sigma(I)]$ (on *F* for obsd reflns)[a]	0.0373
w$R_2[I > 2\sigma(I)]$ (on F^2 for all reflns)[b]	0.0866
Goodness-of-fit on F^2	1.019
Largest diff. peak and hole	0.334 and −0.273 e.Å^{-3}

[a] $R_1 = \Sigma \mathrm{I}\,\mathrm{I}F_o\mathrm{I} - \mathrm{I}F_c\mathrm{I}\,\mathrm{I}/\Sigma\mathrm{I}F_o\mathrm{I}$.
[b] $wR_2 = \{\Sigma[w(F_o^2 - F_c^2)^2]/\Sigma w(F_o^2)^2\}^{1/2}$.

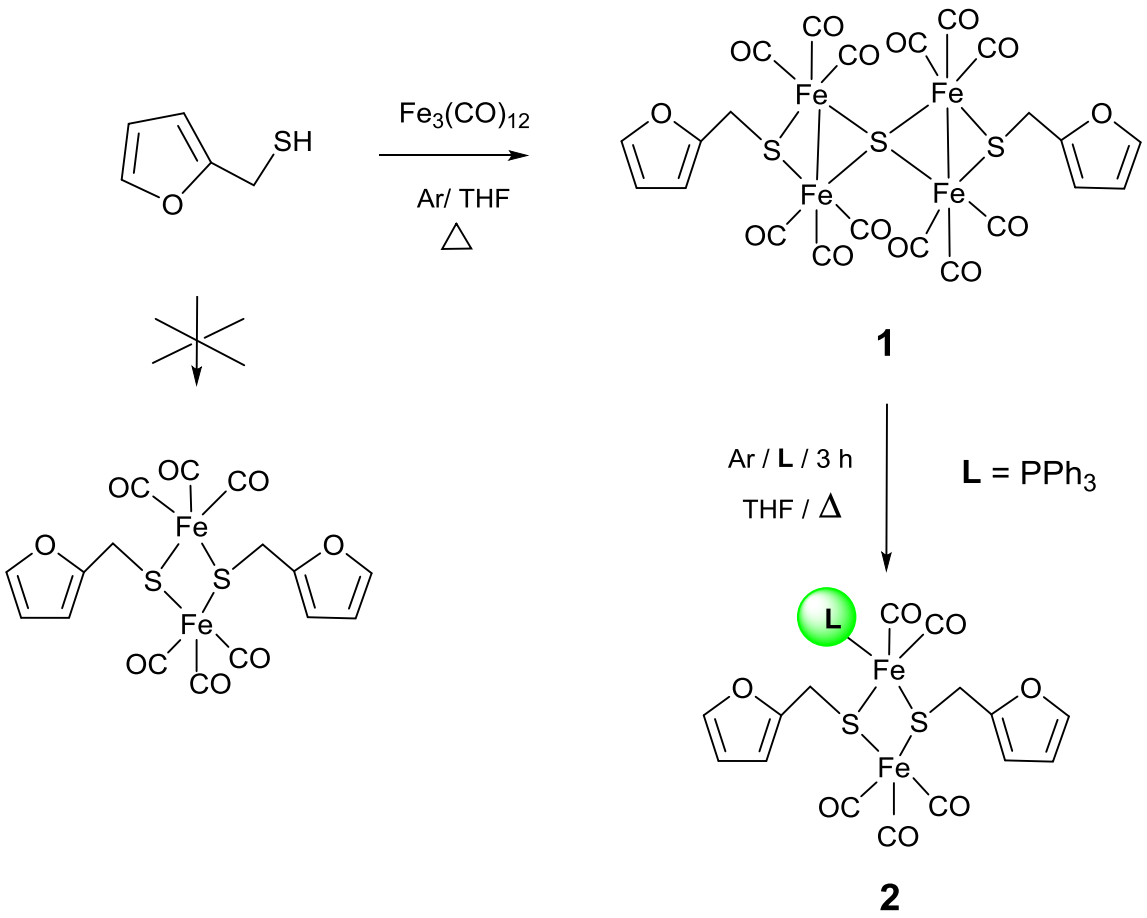

Scheme 1. Synthetic scheme for complexes **1** and **2**.

3.3 *FTIR spectral studies*

The complexes were characterized by different spectroscopic techniques. The FTIR spectra for the complexes were recorded in both dichloromethane and acetonitrile (Table 3 and Figures S4–S5, Supplementary Information). For the tetranuclear iron complex, the CO stretching frequencies were observed between 2070 and 1970 cm^{-1}. The peaks correspond to the terminal carbonyl ligands. On the other hand, the phosphine substituted complex **2** displayed peaks at lower wavenumbers (shifted by 30 cm^{-1}) in comparison to complex **1**. The attachment of electron-donating triphenylphosphine ligand at the apical position on one of the iron centers leads to lower terminal CO stretching frequencies.

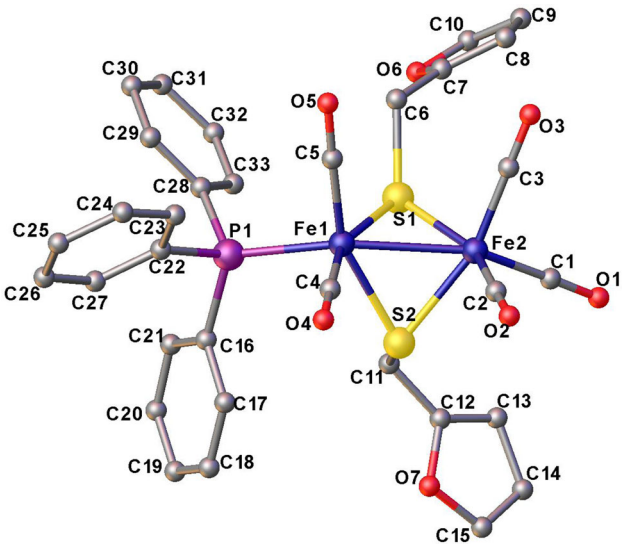

Figure 2. Molecular structure of [Fe_2(μ-2-furylmethanethiolate)$_2$(CO)$_5$(PPh_3)] **2**. Hydrogen atoms have been omitted for clarity.

3.4 *NMR spectroscopy*

The ^{1}H NMR spectrum of complex **2** in $CDCl_3$ displayed peaks in the range 7.70–7.30 ppm corresponding to the phenyl ring protons of the PPh_3 ligand (Figure S6, Supplementary Information). The peaks between 6.22 and 5.78 ppm were due to the protons present in the two furyl rings (3 protons in each ring). The peaks between 3.43 and 2.81 ppm correspond to four protons from the -CH_2- a bridge between sulphur and the furyl ring.

Table 2. Selected bond lengths (Å) and angles (°) for complex **2**.

Bond lengths		Bond angles	
Fe(1)–Fe(2)	2.5207(4)	Fe(1)–S(2)–Fe(2)	67.600 (19)
Fe(1)–S(1)	2.2518(6)	Fe(1)–S(1)–Fe(2)	67.772 (18)
Fe(1)–S(2)	2.2646(6)	S(2)–Fe(2)–Fe(1)	56.162 (17)
Fe(2)–S(1)	2.2691(6)	S(2)–Fe(1)–Fe(2)	56.238 (17)
Fe(2)–S(2)	2.2666(6)	S(1)–Fe(2)–Fe(1)	55.788 (16)
Fe(1)–P(1)	2.2344(6)	S(1)–Fe(1)–Fe(2)	56.440 (17)
Fe(1)–C(4)	1.772(2)	S(2)–Fe(2)–S(1)	79.90 (2)
Fe(1)–C(5)	1.760(2)	S(1)–Fe(1)–S(2)	80.32 (2)
Fe(2)–C(1)	1.801(3)	C(4)–Fe(1)–S(1)	158.89 (8)
Fe(2)–C(2)	1.787(3)	C(4)–Fe(1)–S(2)	87.00 (8)
Fe(2)–C(3)	1.767(3)	C(5)–Fe(1)–S(1)	91.94 (7)
C(1)–O(1)	1.139(3)	C(5)–Fe(1)–S(2)	157.27(8)
C(2)–O(2)	1.131(3)	C(5)–Fe(1)–Fe(2)	101.72 (8)
C(3)–O(3)	1.136(3)	C(5)–Fe(1)–C(4)	93.40 (10)
C(4)–O(4)	1.137(3)	C(4)–Fe(1)–P(1)	95.92 (8)
C(5)–O(5)	1.146(3)	C(5)–Fe(1)–P(1)	96.53 (8)
		P(1)–Fe(1)–S(1)	103.74 (2)
		P(1)–Fe(1)–S(2)	106.04 (2)
		P(1)–Fe(1)–Fe(2)	153.12 (2)
		C(1)–Fe(2)–S(1)	105.92 (9)
		C(1)–Fe(2)–Fe(1)	149.94 (8)
		C(2)–Fe(2)–Fe(1)	96.85 (9)
		C(3)–Fe(2)–Fe(1)	105.16 (10)
		C(1)–Fe(2)–S(2)	100.07 (9)
		C(2)–Fe(2)–S(2)	87.91 (8)
		C(3)–Fe(2)–S(2)	160.91 (10)
		C(2)–Fe(2)–C(1)	100.59 (12)
		C(3)–Fe(2)–C(1)	98.88 (13)
		C(3)–Fe(2)–C(2)	90.91 (13)

The ^{31}P $\{^{1}H\}$ NMR spectrum of complex **2** displayed a peak at 59.8 ppm due to the presence of the PPh_3 ligand at one of the iron centers. In addition, a small peak at 53.98 ppm is probably due to the presence of an isomer for complex **2** (Figure S7, Supplementary Information). This could be due to the axial/equatorial or axial/axial orientation of the two furyl rings.

3.5 *UV-visible absorption spectroscopy*

For complexes **1** and **2**, the electronic effect of the monothiolate ligands and the monodentate phosphine ligand on the iron centers was elucidated from the measured UV-Vis absorption spectra in acetonitrile (Figure 3). The spectra of both the complexes displayed two absorption bands at 332 (46,000), 468 (6200) and 372 (17,000), 505 (2400) nm (M^{-1} cm^{-1}) for **1** and **2**, respectively. The peaks in the UV region were due to $\pi - \pi^*$ electronic transitions while those in the visible region can be assigned as d-d transitions. The significant similarity between the UV–Vis spectra of complexes **1** and **2** suggests that there is very little difference of the influence of the monothiolate and phosphine ligands on the resultant $Fe(CO)_6$ and $Fe(CO)_5$ cores.

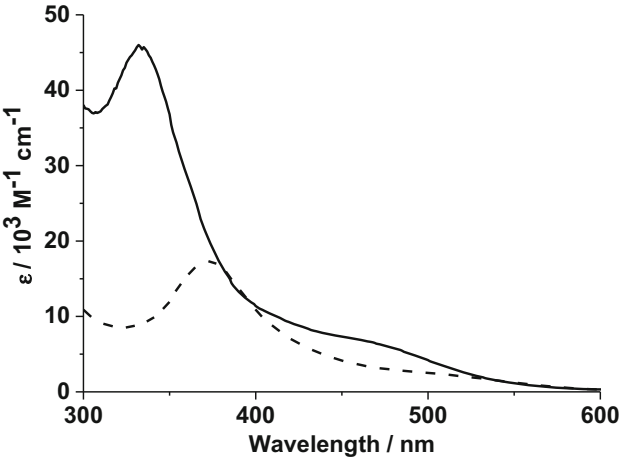

Figure 3. UV-Vis spectra for complexes **1** (—-) and **2** (---) in acetonitrile.

3.6 *Electrochemistry*

The cyclic voltammograms (CVs) for complexes **1** and **2** were measured in acetonitrile under an argon atmosphere (Figure 4 and Table 4). The CVs for **1** displayed two one-electron irreversible reduction waves (E_{pc} = −1.80 and –2.53 V *vs.* Fc/Fc^+) that can be assigned as $Fe^IFe^I \rightarrow Fe^IFe^0$ and $Fe^IFe^0 \rightarrow Fe^0Fe^0$ redox processes (Figure 4). One-electron irreversible oxidation for **1** was observed at 0.70 V which can be ascribed as $Fe^IFe^I \rightarrow Fe^IFe^{II}$. The reduction of compound **2** occurred at $E_{pc} = -1.92$, and its oxidation at 0.36 V. Substitution of one CO ligand in **1** with PPh_3 led to a more electron-rich Fe center in **2**, hence leading to more negative first reduction potential and less

Table 3. FTIR data for complexes **1** and **2**.

Complex	Wavenumber/cm^{-1}	
	Dichloromethane	Acetonitrile
1	2070 (s), 2027 (s), 1968 (br)	2069 (s), 2036 (s), 1988 (br)
2	2041 (s), 1979 (m), 1960 (s), 1926 (s)	2033 (s), 1980 (m), 1953 (s), 1918 (s)

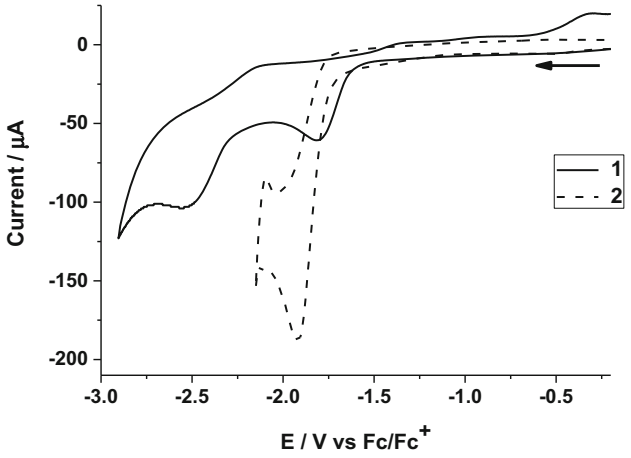

Figure 4. Cyclic voltammograms for 1 mM of complexes **1** (—) and **2** (----) in acetonitrile at a scan rate of 0.1 Vs^{-1}.

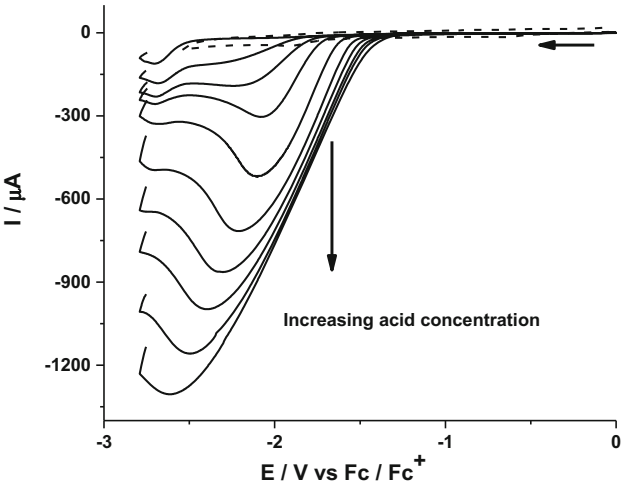

Figure 5. Cyclic voltammograms for complex **2** (1 mM) in CH_3CN in the absence (---) and presence of increasing amounts (6.95, 34.45, 61.53, 88.19, 133.84, 196.81, 257.78, 316.36, 372.86, 453.91 mM) of acetic acid (—) at a scan rate of 0.1 Vs^{-1}.

positive oxidation for complex **2**. Both the complexes were examined as electrocatalysts for the reduction of protons to molecular hydrogen in the presence of acetic and trifluoroacetic (TFA) acids. The complexes were found to be more efficient catalysts in presence of TFA which is a moderately strong acid in comparison to acetic acid. The complexes were also found to be active catalysts in the presence of perchloric acid, however, the catalytic currents were lower and diminished with the addition of about 15 mM of acid.

CVs of **1** and **2** in the presence of acetic acid showed new peaks at −2.33 and −2.18 V, respectively, *vs.* Fc/Fc^+ which shifted to more negative potentials with an increase in the amount of acid (Figure 5 and Figure S8, Supplementary Information). The increase of current at this reduction potential with the increase in the amount of acid can be attributed to the reduction of protons to molecular hydrogen.[28] For complex **1,** an additional reduction peak was observed at –1.48 V the peak current for which did not increase with the addition of increasing amounts of acid. This additional peak was absent for complex **2**.

The background current due to direct reduction of protons at the glassy carbon electrode without catalyst in the presence of the two different acids were found to be negligible for potentials in the range –1.0 to –2.5 V.[29] Hence, the acid-induced current in the presence of catalysts can be attributed to catalytic turnover **1** and **2** showed comparable electrocatalytic activity. The catalytic currents were, however, much higher than the recently reported complexes $[Fe_2(\mu\text{-}p\text{-toluenethiolate})_2(CO)_6]$, $[Fe_2(\mu\text{-}CH_2Ph)_2(CO)_6]$ and $[\mu_4\text{-}S(\mu_2\text{-}(\alpha\text{-toluenethiolate})Fe_2(CO)_6)_2]$.[9b] Also the electrocatalytic proton reduction for these reported complexes was studied in dichloromethane. The CVs for **1** in the presence of TFA initially displayed a peak at –1.47 V (Figure S9, Supplementary Information). On addition of 48 mM of acid two

Table 4. Electrochemical data for complexes **1** and **2** in acetonitrile.

Complex	E_{pc}/V	E_{cat}/V AcOH	E_{cat}/V TFA	Overpotential/V	
				AcOH	TFA
1	−1.80 −2.53	−2.33	−1.47	−0.87	−0.58
$[\mu_4\text{-}S(\mu_2\text{-}(\alpha\text{-toluenethiolate})Fe_2(CO)_6)_2]^{a,b}$	−1.48 −1.86	−1.96	–	–	–
2	−1.92	−2.18	−1.70	−0.72	−0.81
$[Fe_2(\mu\text{-}SPh)_2(CO)_6]^c$	−1.44	−2.26	–	−0.80	–
$[Fe_2(\mu\text{-napthalene-2-thiolate})_2(CO)_6]^d$	−1.33	−2.00	–	−0.54	–
$[Fe_2(\mu\text{-napthalene-2-thiolate})_2(CO)_5PPh_3]^d$	−1.49	−1.97	–	−0.51	–

[a]In CH_2Cl_2 *vs.* Ag/AgCl; [b]Ref.[9b]; [c]Ref.[11]; [d]Ref.[9a]

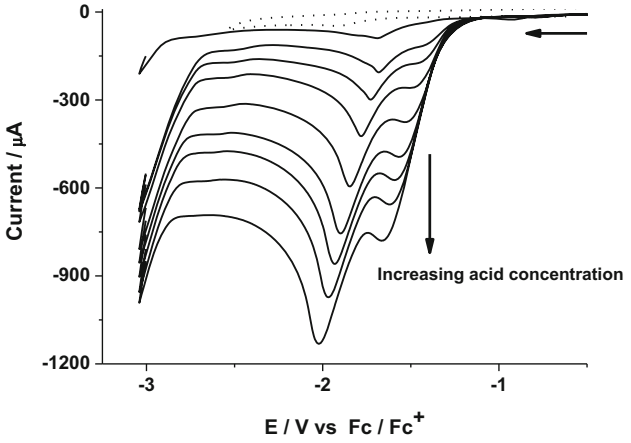

Figure 6. Cyclic voltammograms for complex **2** (1 mM) in CH_3CN in the absence (---) and presence of increasing amounts of TFA (4.76, 10.61, 15.20, 23.08, 33.96, 44.44, 54.54, 64.28, 78.26 mM) (—) at a scan rate of 0.1 Vs^{-1}.

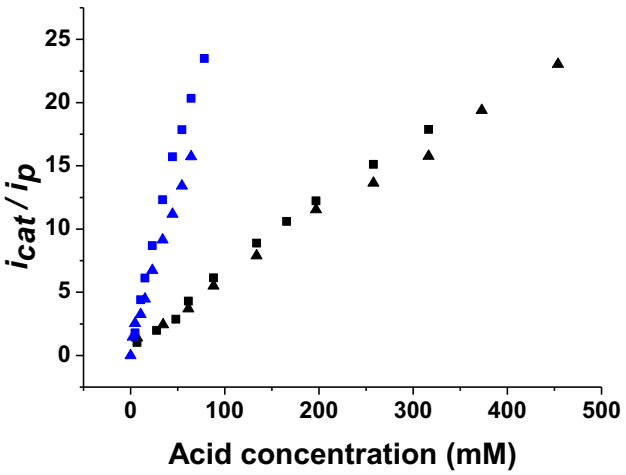

Figure 7. Plot of i_{cat}/i_p *vs.* acid concentration for complexes **1** (■) and **2** (▲) (1 mM) in presence of acetic acid (black); and for the second reduction peak of complexes **1** (■) and **2** (▲) (1 mM) in presence of TFA (blue) at a scan rate of 0.1 Vs^{-1}.

peaks were observed at –1.56 and –1.71 V. These two peaks shifted cathodically and the current height for all the peaks increased with increase in the amount of acid. A tetra-nuclear iron complex [μ_4-S(μ_2-(α-toluenethiolate)$_2$Fe$_2$(CO)$_6$] similar to complex **1** has been reported recently as a catalyst for proton reduction in dichloromethane (Table 4).[9b] A few other tetranuclear complexes reported earlier with di- and tetra-thiolate linkers displayed lower catalytic currents.[30–38] However, the catalytic currents for the reported complex [μ_4-S(μ_2-(α-toluenethiolate)$_2$Fe$_2$(CO)$_6$] were lower than complex **1**.[9b] On the other hand, complex **2** displayed a peak at –1.70 V on the addition of TFA. A second peak was observed at –1.43 V, after addition of about 10 mM of acid (Figure 6). These two peaks shifted cathodically and the current height for all the peaks increased with increase in the amount of acid. The plots of i_{cat}/i_p *vs.* acid concentration for complexes **1** and **2** in presence of two different acids are shown in Figure 7 (Figure S10, Supplementary Information). The overpotential for **2** in acetic acid was found to be lower than those of complexes **1** and [$Fe_2(\mu$-SPh)$_2$(CO)$_6$] while it was higher than complex **1** in presence of TFA (Table 4).[11,28] The catalytic rate of proton reduction was investigated by using the following equation:

$$\frac{i_{\text{cat}}}{i_{\text{p}}} = \frac{n}{0.446}\sqrt{\frac{RTk_{\text{obs}}}{Fv}}$$

where i_{cat} is the catalytic current, i_p is the peak current measured in the absence of acid, n is the number of electrons involved in the catalytic reaction, k_{obs} is the observed first-order rate constant, R is the ideal gas constant, T is the temperature in Kelvin, F is Faraday's constant, v is the scan rate. For complexes **1** and **2**, it was observed that k_{obs} increased linearly with acid concentration, which suggests a first-order dependence of the catalytic rate on acid concentration (Figures S11–S12, Supplementary Information).[39–42]

The catalytic efficiency (C.E.) for complexes **1** and **2** in AcOH and TFA was calculated using the method defined by Felton and co-workers,[28] C.E. = $(i_{cat}/i_d)/(C_{HA}/C_{cat})$($i_{cat}$ = catalytic current, i_d = current for reduction of catalyst in absence of acid, C_{HA} = concentration of acid, C_{cat} = concentration of catalyst). The values of C.E. of **1** and **2** vary in the range 0.34 to 0.11 (for **1**) and 0.25 to 0.19 (for **2**) in acetic acid, and 0.77 to 0.54 (for **1**) and 0.71 to 0.51 (for **2**) in TFA, decreasing with increasing acid concentration.

4. Conclusions

In summary, a new diiron carbonyl complex **2** was prepared from the tetranuclear precursor complex **1** using the monodentate phosphine ligand (PPh_3). The electrochemical investigations of complexes **1** and **2** were performed in acetonitrile in the presence of acetic acid and TFA. Complexes **1** and **2** were found to show comparable catalytic activity for proton reduction to dihydrogen. The reduction potential for complex **1** in the presence of TFA appeared at more negative potential than that observed for **2**. However, in the presence of acetic acid, the reduction potentials were comparable. Also, the complexes were more efficient catalysts in presence of stronger acids.

Supplementary Information (SI)

The supplementary information includes X-ray, FTIR, NMR and electrochemical data. CCDC reference numbers 1519040 (for **1**) and 1442928 (for **2**) contain the supplementary crystallographic data for this paper. Copies of this information are available on request at free of charge from CCDC, Union Road, Cambridge, CB21EZ, UK (fax: +44-1223-336-033; E-mail: deposit@ccdc.ac.uk or http://www.ccdc.cam.ac.uk). Supplementary Information is available at www.ias.ac.in/chemsci.

Acknowledgements

Financial support from the Department of Science & Technology (DST), India (SR/S1/IC-28/2011) is gratefully acknowledged. SKG is thankful to the University of Delhi, India for providing R&D grant. MN is grateful to Council of Scientific & Industrial Research (CSIR) and VK and NK are grateful to University Grant Commissions (UGC) for fellowship.

References

1. (a) Evans D J and Pickett C J 2003 Chemistry and the hydrogenases *Chem. Soc. Rev.* **32** 268; (b) Lubitz W, Ogata H, Rüdiger O and Reijerse E 2014 hydrogenases *Chem. Rev.* **114** 4081; (c) Wittkamp F, Senger M, Stripp S T and Apfel U-P 2018 [FeFe]-hydrogenases: recent developments and future perspectives *Chem. Commun.* **54** 5934
2. Peters J W, Lanzilotta W N, Lemon B J and Seefeldt L C 1998 X-ray crystal structure of the Fe-only hydrogenase (CpI) from *Clostridium pasteurianum* to 1.8 angstrom resolution *Science* **282** 1853
3. Nicolet Y, Piras C, Legrand P, Hatchikian C E and Juan Fontecilla-Camps C 1999 *Desulfovibrio desulfuricans* iron hydrogenase: the structure shows unusual coordination to an active site Fe binuclear center *Structure* **7** 13
4. Ryde U, Greco C and Gioia L D 2010 Quantum refinement of [FeFe] hydrogenase indicates a dithiomethylamine ligand *J. Am. Chem. Soc.* **132** 4512
5. Barton B E, Olsen M T and Rauchfuss T B 2008 Aza- and oxadithiolates are probable proton relays in functional models for the [FeFe]-hydrogenases *J. Am. Chem. Soc.* **130** 16834
6. (a) Lewis N S and Nocera D G 2006 Powering the planet: chemical challenges in solar energy utilization *Proc. Natl. Acad. Sci.* **103** 15729; (b) Fontecilla-Camps J C, Volbeda A,Cavazza C and Nicolet Y 2007 Structure/function relationships of [NiFe]- and [FeFe]-hydrogenases *Chem. Rev.* **107** 4273
7. (a) Navarro R M, Sánchez M C S, Galvan M C A, Valle F D and Fierro J L G 2009 Hydrogen production from renewable sources: biomass and photocatalytic opportunities *Energy Environ. Sci.* **2** 35; (b) Schilter D, Camara J M, Huynh M T, Hammes-Schiffer S and Rauchfuss T B 2016 Hydrogenase enzymes and their synthetic models: the role of metal hydrides *Chem. Rev.* **116** 8693; (c) Li Y and Rauchfuss T B 2016 Synthesis of diiron(I) dithiolato carbonyl complexes *Chem. Rev.* **116** 7043; (d) Wang N, Wang M, Chen L and Sun L 2013 Reactions of [FeFe]-hydrogenase models involving the formation of hydrides related to proton reduction and hydrogen oxidation *Dalton Trans.* **42** 12059; (e) Tschierlei S, Ott S and Lomoth R 2011 Spectroscopically characterized intermediates of catalytic H_2 formation by [FeFe] hydrogenase models *Energy Environ. Sci.* **4** 2340; (f) Simmons T R, Berggren G, Bacchi M, Fontecave M and Artero V 2014 Mimicking hydrogenases: from biomimetics to artificial enzymes *Coord. Chem. Rev.* **270–271** 127; (g) Zhao P-H, Ma Z-Y, Hu M-Y, He J, Wang Y-Z, Jing X-B, Chen H-Y Wang Z and Li Y-L 2018 PNP-chelated and -bridged diiron dithiolate complexes $Fe_2(\mu\text{-pdt})(CO)_4\{(Ph_2P)_2NR\}$ together with related monophosphine complexes for the $[2Fe]_H$ subsite of [FeFe]-hydrogenases: preparation, structure, and electrocatalysis *Organometallics* **37** 1280; (h) Rauchfuss T B 2015 Diiron azadithiolates as models for the [FeFe]-hydrogenase active site and paradigm for the role of the second coordination sphere *Acc. Chem. Res.* **48** 2107; (i) Berggren G, Adamska A, Lambertz C, Simmons T R, Esselborn J, Atta M, Gambarelli S, Mouesca J M, Reijerse E, Lubitz W, Happe T, Artero V and Fontecave M 2013 Biomimetic assembly and activation of [FeFe]-hydrogenases *Nature* **499** 66; (j) Weber K, Weyhermüller T, Bill E, Erdem Ö F and Lubitz W 2015 Design and characterization of phosphine iron hydrides: toward hydrogen-producing catalysts *Inorg. Chem.* **54** 6928
8. (a) Pandey I K, Natarajan M and Kaur-Ghumaan S 2015 Hydrogen generation: aromatic dithiolate-bridged metal carbonyl complexes as hydrogenase catalytic site models *J. Inorg. Biochem.* **143** 88; (b) Tard C and Pickett C J 2009 Structural and functional analogues of the active sites of the [Fe]-, [NiFe]- and [FeFe]-hydrogenases *Chem. Rev.* **109** 2245; (c) Wang M, Chen L, Li X and Sun L 2011 Approaches to efficient molecular catalyst systems for photochemical H_2 production using [FeFe]-hydrogenase active site mimics *Dalton Trans.* **40** 12793; (d) Makouf N B, Mousser H B, Darchen A and Mousser A 2018 Carbon monoxide substitutions by trimethyl phosphite in diiron dithiolate complex: Fe-Fe bond cleavage, selectivity of the substitutions, crystal structures and electrochemical studies *J. Organomet. Chem.* **866** 35; (e) Li Y-L, Ma Z-Y, He J, Hu M-Y and Zhao P-H 2017 Aminophosphine-substituted diiron dithiolate complexes: synthesis, crystal structure, and electrocatalytic investigation *J. Organomet. Chem.* **851** 14; (f) Song L-C, Gu Z-C, Zhang W-W, Li Q-L, Wang Y-X and Wang H-F 2015 synthesis, structure, and electrocatalysis of butterfly $[Fe_2SP]$ cluster complexes relevant to [FeFe]- hydrogenases *Organometallics* **34** 4147; (g) Ghosh S, Rahaman A, Holt K B, Nordlander E, Richmond M G, Kabir S E and Hogarth G 2016 Hydrogenase biomimetics with redox-active ligands: electrocatalytic proton reduction by $[Fe_2(CO)_4(\kappa^2\text{-diamine})(\mu\text{-edt})]$ (diamine = 2,2′-bipy, 1,10-phen) *Polyhedron* **116** 127; (h) Ahmed Md E, Dey S and Dey A 2017 H_2 evolution catalyzed by a FeFe-hydrogenase synthetic model

covalently attached to graphite surfaces *Chem. Comm.* **53** 8188; (i) Durgaprasad G and Das S K 2015 Modelling the active site of [FeFe]-hydrogenase: electrocatalytic hydrogen evolution from acetic acid catalysed by $[Fe_2(\mu\text{-L})(CO)_6]$ and $[Fe_2(\mu\text{-L})(CO)_5(PPh_3)]$ (L = pyrazine-2,3-dithiolate, quinoxaline-2,3-dithiolate and pyrido[2,3-b]pyrazine-2,3-dithiolate) *J. Chem. Sci.* **127** 295

9. (a) Mebi C A, Karr D S and Noll B C 2013 Using naphthalene-2-thiolate ligands in the design of hydrogenase models with mild proton reduction overpotentials *Polyhedron* **50** 164; (b) Haley A L, Broadbent L N, McDaniel L S, Heckman S T, Hinkle C H, Gerasimchuk N N, Hershberger J C and Mebi C A 2013 [Fe–Fe] hydrogenase models: iron(I)-carbonyl clusters coupled to alpha- and para-toluenethiolate ligands *Polyhedron* **114** 218
10. Tang Y, Wei Z, Zhong W and Liu X 2011 Diiron complexes with pendant phenol group(s) as mimics of the diiron subunit of [FeFe]-hydrogenase: synthesis, characterisation and electrochemical investigation *Eur. J. Inorg. Chem.* 1112
11. Si Y, Hu M and Chen C 2008 Diiron models for active site of FeFe-hydrogenase with aromatic thiolate bridges: Structures and electrochemistry *C. R. Chim.* **11** 932
12. Yu Z, Wang M, Li P, Dong W, Wang F and Sun L 2006 Diiron dithiolate complexes containing intra-ligand $NH\cdots S$ hydrogen bonds: [FeFe] hydrogenase active site models for the electrochemical proton reduction of HOAc with low overpotential *Dalton Trans.* 2400
13. Chong D, Georgakaki I P, Rodriguez R M, Chinchilla J S, Soriaga M P and Darensbourg M Y 2003 Electrocatalysis of hydrogen production by active site analogues of the iron hydrogenase enzyme: structure/function relationships *Dalton Trans.* 4158
14. Shi Y C, Tan H and Shi Y 2014 Synthesis and stereochemistry of diiron complexes generated from the reactions of iron carbonyls with 2-thienyl thiol and 2-thienyl methanethiol *Polyhedron* **67** 218
15. In-noi O, Haller K J, Hall, Brezinski W P, Marx J M, Sakamoto T, Evans D H, Glass R S and Lichtenberger D L 2014 Electrochemical, spectroscopic, and computational study of bis(μ-methylthiolato)diironhexacarbonyl: homoassociative stabilization of the dianion and a chemically reversible reduction/reoxidation cycle *Organometallics* **33** 5009
16. Long L, Jiang X, Wang X, Xiao Z and Liu X 2013 Water-soluble diiron hexacarbonyl complex as a CO-RM: controllable CO-releasing, releasing mechanism and biocompatibility *Dalton Trans.* **42** 15663
17. Karslyan E E, Shul'pina L S, Kozlov Y N, Pombeiro A J L and Shul'pin G B 2013 Oxygenation of saturated and aromatic hydrocarbons withH_2O_2 catalysed by the carbonyl thiophenolate iron complex$(OC)_3Fe(PhS)_2Fe(CO)_3$ *Catal. Today* **218–219** 93
18. Hogarth G, Richards I and Subasi E 2008 γ-Hydroxypropyl-functionalised iron thiolate complexes: crystal and molecular structure of $[\{Fe_2(CO)_6(\mu\text{-}SCH_2CH_2CH_2OH)\}_2(\mu_4\text{-S})]$ *Transit. Met. Chem.* **33** 729
19. Liaw W F, Tsai W T, Gau H B, Lee C M, Chou S Y, Chen W Y and Lee G H 2003 Dinuclear iron(II)-cyanocarbonyl complexes linked by two/three bridging ethylthiolates: relevance to the active site of [Fe] hydrogenases *Inorg. Chem.* **42** 2783
20. Delgado E, Hernandez E, Mansilla N, Zamora F and Cruz L A M 1999 Iron carbonyls with bulky thiolate ligands: crystal structures of $[Fe_2(CO)_6(\mu\text{-}SC_6H_2i_{Pr3}\text{-}2,4,6)_2]$ and $(C_6H_2i_{Pr3}-2,4,6)2S_2$ *Inorg. Chim. Acta* **284** 14
21. Han C, Huang X N, Guo Y L and Liu W 2010 μ_4-Sulfidobis(μ-2-furylmethanethiolato)bis[tricarbonyliron](Fe—Fe) *Acta Cryst.* **E66** m820
22. Sheldrick G M 2015 Crystal structure refinement with SHELXL *Acta Cryst.* **71** 3
23. Sheldrick G M 1997 *SHELX-97: Programs for crystal structure solution and refinement.* University of Göttingen, Göttingen, Germany
24. Sheldrick G M 1990 Phase annealing in SHELX-90: direct methods for larger structures *Acta Cryst.* **A46** 467
25. Farrugia L J 2012 WinGX and ORTEP for Windows: an update *J. Appl. Cryst.* **45** 849
26. Dolomanov O V, Bourhis L J, Gildea R J, Howard J A K and Puschmann H 2009 OLEX2: a complete structure solution, refinement and analysis program *J. Appl. Cryst.* **42** 339
27. Nicolet Y, de Lacey A L, Vernéde X, Fernandez V M, Hatchikian E C and Fontecilla Camps J C 2001 Crystallographic and FTIR spectroscopic evidence of changes in Fe coordination upon reduction of the active site of the Fe-only hydrogenase from *Desulfovibrio desulfuricans* *J. Am. Chem. Soc.* **123** 1596
28. (a) Felton G A N, Mebi C A, Petro B J, Vannucci A K, Evans D H, Glass R S and Lichtenberger D L 2009 Review of electrochemical studies of complexes containing the Fe_2S_2 core characteristic of [FeFe] hydrogenases including catalysis by these complexes of the reduction of acids to form dihydrogen *J. Organomet. Chem.* **694** 2681; (b) Felton G A N, Glass R S, Lichtenberger D L and Evans D H 2006 Iron-only hydrogenase mimics. Thermodynamic aspects of the use of electrochemistry to evaluate catalytic efficiency for hydrogen generation *Inorg. Chem.* **45** 9181
29. McCarthy B D, Martin D J, Rountree E S, Ullman A C and Dempsey J L 2014 Electrochemical reduction of brønsted acids by glassy carbon in acetonitrile-implications for electrocatalytic hydrogen evolution *Inorg. Chem.* **53** 8350
30. Apfel U P, Halpin Y, Görls H, Vos J G, Schweizer B, Linti G and Weigand W 2007 Synthesis and characterization of hydroxy-functionalized models for the active site in Fe-only-hydrogenases *Chem. Biodivers.* **4** 2138
31. Chen L, Wang M, Gloaguen F, Zheng D, Zhang P and Sun L 2013 Tetranuclear iron complexes bearing benzenetetrathiolate bridges as four-electron transformation templates and their electrocatalytic properties for proton reduction *Inorg. Chem.* **52** 1798
32. Chen L, Wang M, Gloaguen F, Zheng D, Zhang P and Sun L 2012 Multielectron-transfer templates via consecutive two-electron transformations: iron–sulfur complexes

relevant to biological enzymes *Chem. Eur. J.* **18** 13968

33. Karnahl M, Orthaber A, Tschierlei S, Nagarajan L and Ott S 2012 Structural and spectroscopic characterization of tetranuclear iron complexes containing a $P_2^R N_2^{Ph}$ bridge *J. Coord. Chem.* **65** 2713
34. Liu X F, Yu X Y and Gao H Q 2014 Reactions of cluster complex triiron enneacarbonyl disulfide with phosphine ligands *Mol. Cryst. Liq. Cryst.* **592** 229
35. Song L C, Gong F H, Meng T, Ge J H, Cui L N and Hu Q M 2004 General synthetic route to double-butterfly Fe/S cluster complexes via reactions of the dianions $\{[(\mu\text{-CO})Fe_2(CO)_6]_2(\mu\text{-SZS-}\mu)\}^{2-}$ with electrophiles *Organometallics* **23** 823
36. Song L C, Gao J, Wang H T, Hua Y J, Fan H T, Zhang X Gand Hu Q M 2006 Synthesis and structural characterization of metallocrown ethers containing butterfly Fe_2S_2 cluster cores. Biomimetic hydrogen evolution catalyzed by $Fe_2(\mu\text{-}SCH_2CH_2OCH_2CH_2S\text{-}\mu)(CO)_6$ *Organometallics* **25** 5724
37. Teo B K, Wudl F, Hauser J J and Kruger A 1977 Reactions of tetrathionaphthalene with transition metal carbonyls. Synthesis and characterization of two new organometallic semiconductors $(C_{10}H_4S_4Ni)_x$ and $[C_{10}H_4S_4Co_2(CO)_2]_x$ and a tetrairon cluster $C_{10}H_4S_4Fe_4(CO)_{12}$ *J. Am. Chem. Soc.* **99** 4862
38. Liu X, Ibrahim S K, Tard C and Pickett C J 2005 Iron-only hydrogenase: synthetic, structural and reactivity studies of model compounds *Coord. Chem. Rev.* **249** 1641
39. Costentin C, Passard G and Savéant J M 2015 Benchmarking of homogeneous electrocatalysts. Overpotential, turnover frequency, limiting turnover number *J. Am. Chem. Soc.* **137** 5461
40. Artero V and Saveant J M 2014 Toward the rational benchmarking of homogeneous H_2-evolving catalysts *Energy Environ. Sci.* **7** 3808
41. Song L C, Zhu L, Hu F Q and Wang Y X 2017 Studies on chemical reactivity and electrocatalysis of two acylmethyl(hydroxymethyl)pyridine ligand-containing [Fe]- hydrogenase models $(2\text{-}COCH_2\text{-}6\text{-}HOCH_2C_5H_3N)Fe(CO)_2L$ (L = η^1-SCOMe, η^1 -2-SC_5H_4N) *Inorg. Chem.* **56** 15216
42. Hou K, Poh H T and Fan W Y 2014 Electrocatalytic hydrogen generation by a trithiolato-bridged dimanganese hexacarbonyl anion with a turnover frequency exceeding $40\,000 s^{-1}$ *Chem. Commun.* **50** 6630